Assembly of silver nanoparticles on nanowires into ordered nanostructures with femtosecond laser radiation

L. Lin,[1,2] H. Huang,[2] M. Sivayoganathan,[2] L. Liu,[1,*] G. Zou,[1]
W. W. Duley,[2,3] and Y. Zhou[1,2,4]

[1]Department of Mechanical Engineering, Tsinghua University, Beijing 100084, China

[2]Centre for Advanced Materials Joining, University of Waterloo, Ontario N2L 3G1, Canada

[3]Department of Physics and Astronomy, University of Waterloo, Ontario N2L 3G1, Canada

[4]e-mail: nzhou@uwaterloo.ca

*Corresponding author: liulei@mail.tsinghua.edu.cn

In this work, we show that well-ordered structures of silver nanoparticles on nanowire substrates can be produced by irradiation with femtosecond (fs) laser pulses at fluences ranging from 10.3 to 15.9 mJ/cm^2 if the direction of polarization is parallel to the long axis of the nanowire. Experimental results show that a uniformly spaced distribution of nanoparticles is more readily produced on nanowires with lengths L $\leq 2\lambda$, where $\lambda = 800$ nm is the laser wavelength. The distribution of nanoparticles is found to become less well organized as L $\geq 2\lambda$. Finite element method simulations, combined with experimental observations, indicate that nanoparticles are initially distributed in response to the electric field along the clean Ag nanowire arising from optical excitation. This electric field is responsible for the attraction of nanoparticles to certain locations on the nanowire. We show how a fs-laser-driven assembly of nanoparticles on nanowires can be used in the development of a nanoscale optical logic processor. This method of creating periodic arrays of metallic nanoparticles on nanowire substrates then has many possible applications in electro-optics. © 2015 Optical Society of America

OCIS codes: (220.4241) Nanostructure fabrication; (220.4610) Optical fabrication; (250.3750) Optical logic devices; (320.2250) Femtosecond phenomena; (250.5403) Plasmonics.

http://dx.doi.org/10.1364/AO.54.002524

1. Introduction

Metallic nanostructures have become important in nanotechnology because their unique interaction with light is promising for applications such as nanosensors [1], nanoantennas [2], and optical logic circuits [3]. Of the many possible nanostructures, those consisting of nanoparticle–nanowire configurations have received special attention due to high photon–electron coupling efficiency [4,5], leading to potential applications as optical modulators [6]. Nanoparticles–nanowire structures can be produced in various ways including via chemical mixing reactions [7], electron beam lithography [8], and mechanical buckling [6]. However, these methods are often limited by toxicity, high cost, and low efficiency. It is therefore of interest to investigate alternative high-efficiency, low-cost methods for the production of nanoparticle–nanowire structures.

Plasmonic effects offer a promising alternative for the construction of nanoparticle–nanowire structures, since the enhanced optical force associated with plasmon excitation can be used to manipulate nanomaterials. An example occurs with "optical tweezers" which have been successfully used to assemble metal

nanoparticle structures [9–11]. This effect is primarily due to the optically induced electric field along the nanostructures, associated with "hotspots" [12,13]. These "hotspots" can be locally generated along nanowires by optical excitation, providing the possibility to construct nanomaterial structures along nanowires [14,15]. Recently, most work using "hotspots" to trap nano objects has been carried out in solution. This has been driven by many potential applications for the use of this technology in the biological field [9–11]. Despite this interest, only a few studies have concentrated on the trapping of metal nanoparticles in air [16,17]. Using femtosecond (fs) radiation to excite plasmonic nanostructures has been shown to be a promising technique for the enhancement of optical forces [10], and demonstrates that the trapping of nanoparticles by "hotspots" is feasible in air as well as in a solution.

Recent advances in femtosecond laser nanotechnology has focused much attention on 3D micromachining for the fabrication of microfluidic, optofluidic, and electrofluidic devices [18]. Femtosecond laser excitation is also an ideal source for plasmonic nanofabrication, since its high peak intensity can generate strong optical excitation, resulting in strong localized plasmonic fields [19,20]. By applying small particles in this field, force can be generated there, resulting in optical trapping [21,22]. In addition, the nonthermal nature of fs laser excitation minimizes damage and maintains the original part geometry and quality as required for precision fabrication [23]. To date, most studies in this field using fs laser radiation to tailor nanomaterials have focused on the modification of bulk materials by introducing periodic surface structures [24,25]. Few studies have investigated the construction of nanostructures from combinations of nanowires and nanoparticles, as published work has centered on the optimization of joining processes to get bonded structures via plasmonic heating [26,27].

In this article, we show that organized arrays of nanoparticles can be assembled on silver nanowires by controlled irradiation of silver nanoparticle/nanowire composites with 800 nm fs laser radiation. The distribution of self-assembled nanoparticles along the nanowire and the separation between regions of particle concentration has been determined. The origin of this self-assembly in response to the localized electric field generated by optical excitation is also discussed in this paper.

2. Experimental

Silver nanowires (AgNWs) with diameters of 80–100 nm and silver nanoparticles (AgNPs) with sizes of 20–50 nm were synthesized by a modified polyol method as reported before [28]. As-produced nanoparticle and nanowire solutions were centrifuged and then diluted in deionized water. AgNWs and AgNPs composite samples were prepared by sequentially drop-casting these two solutions. An Ag NPs solution was first drop-cast onto a silicon substrate and then dried in a low humidity (30%) air environment for around 10 h. After this, another drop of AgNWs

was added and dried under the same condition. For comparison, another sample containing only AgNWs was also produced using the same method. Samples were irradiated with S-polarized 800 nm laser pulses with a pulse duration of <50 fs generated by a Ti:sapphire laser system. The laser beam was focused to cover a spot of ~4 mm diameter by a convex lens with a 20 cm focal length. The beam was incident perpendicular to the substrate. The repetition rate was 1 kHz and the laser fluence used here was typically 10.3 mJ/cm^2. All experiments were conducted in air. Finite element method (FEM) simulations were carried out using commercial COMSOL MULTIPHYSICS software with a RF module. A scanning electron microscope (SEM, LEO 1550) was used to observe the morphology of the laser-induced nanostructure within the irradiated area on the substrate.

3. Results and Discussion

A. Polarization-Dependent Nanostructure Formation

Figure 1(a) shows an as-produced sample with AgNW and AgNPs deposited on the silicon substrate. It can be seen that small AgNPs are randomly distributed around the wire and no AgNPs are present on the surface of AgNW following deposition. And the AgNW also has a smooth surface. The morphology of the nanowire after laser irradiation was found to depend on the angle between the laser electric field and the direction of the nanowire axis. As shown in Fig. 1(b), the small particles have been moved so that they accumulate all along the side surface of AgNW after fs laser irradiation with the polarized electric field direction perpendicular to the nanowire axis.

When the electric field direction reoriented to be parallel to the long nanowire axis, it is evident that some AgNPs have been attracted to the surface of the AgNW [Fig. 1(c)]. Clusters of AgNPs appear at specific locations on the top and sides of the AgNW. Some locations are spaced ~190 nm apart [see Fig. 1(c)]. This organized structure does not occur when AgNWs without neighboring AgNPs are irradiated by the fs laser under the same conditions [Fig. 1(d)]. This observation suggests that the AgNPs that appear on the AgNW are collected from the surrounding surface. This is apparent as an area exhibiting a lower density of AgNPs is found within about 400 nm of the AgNW [see the dashed lines in Fig. 1(b)]. This occurs for both laser polarization directions.

When the laser polarization direction is not aligned with the long nanowire axis, AgNPs are still attracted to the AgNW (Fig. 2) but their distribution on the wire is less well organized. Unlike irradiation with laser polarization coinciding with the long NW axis [Fig. 1(c)], irradiation with polarizations at angles of 68° and 39° give rise to a less symmetrical distribution of AgNPs (Fig. 2). It is also apparent that AgNPs are now located on the side, as well as on the top surface of the AgNW. This configuration appears in response to the combined effect of the parallel and perpendicular electric field components in
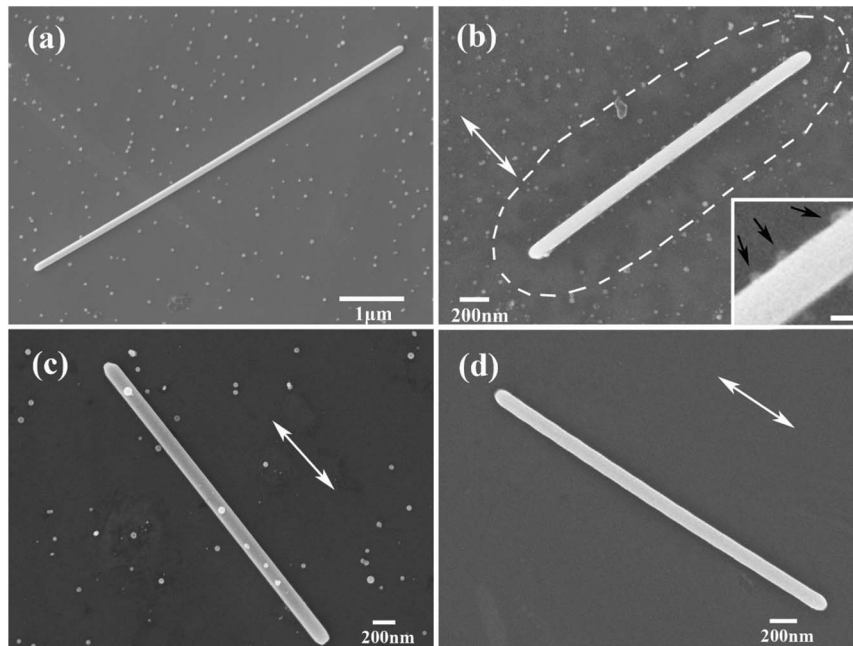
Fig. 1. (a) SEM image of an as-produced sample with AgNW and AgNPs before fs laser irradiation. Samples after laser irradiation for 15 s with the electric field direction perpendicular to the nanowire axis in (b) and parallel to the nanowire axis in (c). Laser fluence: ~10.3 mJ/cm². (d) Sample with only AgNW after laser irradiation for 15 s. The double arrows in (b), (c), and (d) show the polarized electric field direction and the dashed line in (b) shows the area around the silver nanowire has a lower density of nanoparticles. Inset scale in (b): 100 nm, and single arrows show the positions of AgNPs.

the AgNW associated with polarization at a general angle. This indicates that the assembled configuration of AgNPs on the AgNW can be controlled by varying the direction of laser polarization relative to the long axis of the AgNW. It is found that the optimal conditions for producing organized NP structures on AgNWs is obtained with the laser polarization oriented along the long axis of the wire.

Self-organization and the appearance of structure were noticeable when the laser polarization was oriented along the long axis of the AgNW. The resulting NP distribution and the spacing distances between adjacent AgNPs on 28 different AgNWs for parallel polarization were measured and are summarized in Fig. 3. Figure 3(a) shows that NPs tend to be concentrated 110, 210, 300, and 400 nm from one end of the AgNW. These spacing distances are most apparent in AgNWs with lengths less than 1.6 μm [Fig. 3(a)]. And many Ag NPs can also be attached to AgNWs with lengths exceeding 1.6 μm (which is the twice of the wavelength), but in this case the distribution is not as well organized. Figure 3(b) shows particle spacing on three individual AgNWs using data taken from Fig. 3(a). It is evident that the primary separation between adjacent NPs is 190 nm, although a spacing of half and double this amount also occur.

As noted previously in the literature, the electric field generated in nanomaterials under optical excitation is the origin of a trapping force emanating from spaced "hotspots" [29]. Nanoparticles are attracted to these "hotspots" as a result of gradients in the electric field around the nanostructure. The surface plasmon mode in the nanowire gives rise to resonances

according to the relation $L = \left(n + \frac{1}{2}\right)\lambda p$ when the incident laser wavelength is comparable to L, the length of the nanowire, where λp in this expression is the surface plasmon wavelength, and n is an integer [30]. This periodicity is also observed in the experimental data [15]. As previously noted [31], the wave vector at the interface is proportional to the square of the relative permittivity. Variation of the incident wavelength can then be used to change the periodicity. Using optical constants for Ag obtained by Johnson and Christy [32], the surface plasmon wavelength in a silver nanowire surrounded by silicon under 800 nm laser excitation is calculated to be ~380 nm. The separation between intensity peaks will be half this value, i.e., ~190 nm. This is partially consistent with the observed periodicity shown in Fig. 3(b), and is also supported by FEM simulations to be discussed later.

Nanocurrents along the Ag nanowire stimulated by incident laser radiation are a function of the wire–substrate morphology and the dielectric medium surrounding the wire. When a nanowire is supported on a substrate, the plasmon modes have different spatial distributions at the nanowire–air and nanowire–substrate interfaces. This is accompanied by distinct spatial distributions of the charge polarization and the plasmon resonance peaks [12]. In assemblies of metal NPs, near-field coupling between plasmon modes in adjacent NPs occurs over distances of approximately λ [33]. Because of this effect, coupling occurs between the nanowire and any nanoparticles that are present within this distance adjacent to the wire. This is consistent with the area shown by the dashed lines in Fig. 1(b). As a result, a
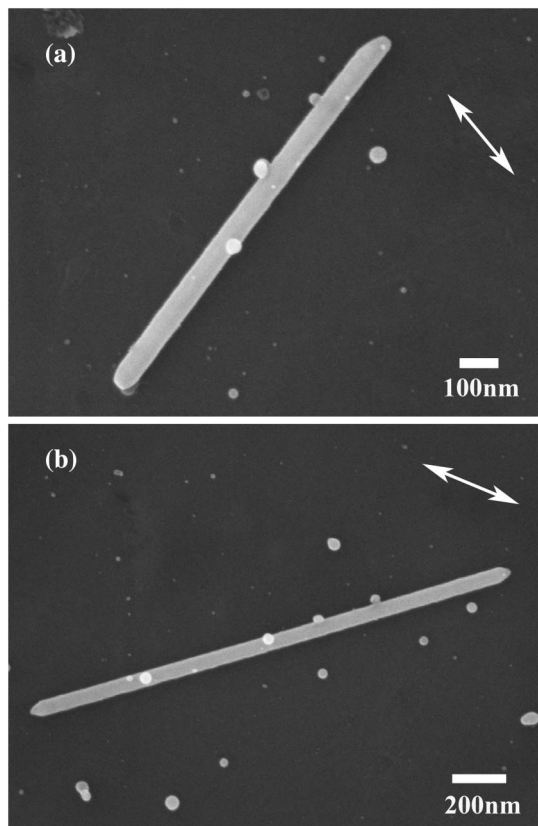
Fig. 2. Polarization dependence of AgNPs assembly on AgNWs. The original samples have a low density of AgNPs. Laser fluence: ∼10.3 mJ/cm². Double arrows in (a) and (b) show the direction of the polarized electric field. The angles, relative to the long axis of the AgNW are 68° in (a) and 39° in (b).
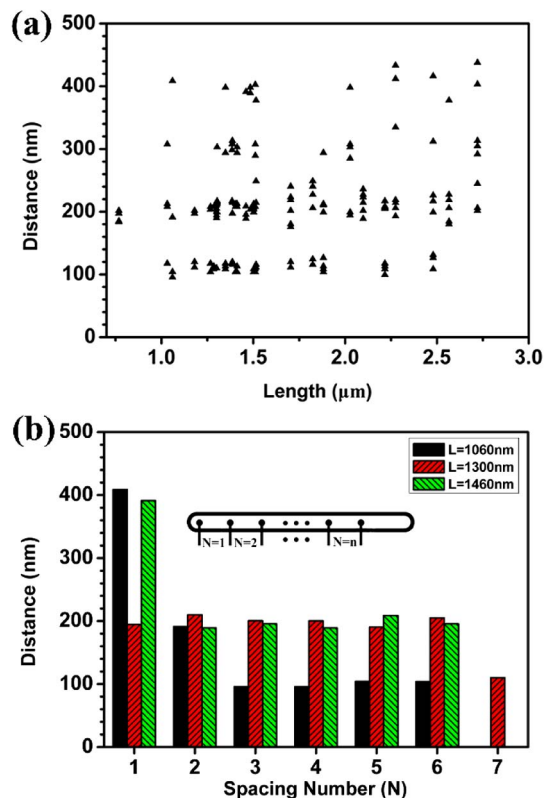

Fig. 3. (a) Summary of the distances between adjacent particles on nanowires with different lengths. The laser electric field direction is parallel to the long axis of the nanowire. Because each wire may contain a different number of nanoparticles, not all distances are present in a given wire–particle combination. (b) Distances between adjacent particles on three specific nanowires. The inset in (b) shows notation for this spacing. For example, N = 2 corresponds to the distance between the second and third nanoparticles counted from one end of the wire.

plasmonic force is generated and NPs are attracted to and assembled on the wire. The final locations of these NPs will be a function of the distribution of "hotspots" around the nanowire.

B. "Hotspot" Distribution by Optical Excitation

Simulations of the electric field were carried out to understand the distribution of "hotspots" at the nanowire–air and nanowire–substrate interfaces. The AgNW has been assigned a length of 2λ where $\lambda = 800$ nm and a diameter of 100 nm. Incident light propagates in the z direction with the polarization direction either parallel or perpendicular to the long axis of the nanowire. The nanowire is placed on a silicon substrate. The resulting electric field distribution when the polarization is along the nanowire is shown in Fig. 4(a). It is apparent that the "hotspots" are distributed along the bottom of the nanowire where it contacts the substrate. The electric field lines associated with these "hotspots" extend into the silicon substrate. The electric field distribution at selected points across the nanowire is shown in the plots labeled a1 and a2 in Fig. 4. At the location of a "hotspot" (a2), a strong electric field is seen to extend around the wire. The field in and on the nanowire is much weaker between "hotspots" (section a1). Ploschner et al. [29] has shown that the plasmonic

electric field will cause small particles to move along the electric field lines toward the wire. However, nanoparticles are not attracted to the lower surface of the wire because the field lines at this location extend into the silicon substrate rather than to points on the surface distant from the wire where particles are present. Thus, the nanoparticles on the silicon surface away from the wire only detect field lines that extend back to the sides and upper surface of the wire. This field can result in a trapping force on the AgNPs that directs them to locations on the top and side surfaces of the nanowire where the electric field is the strongest [29,34]. For this reason, nanoparticles are initially located as in Fig. 1(c). Figure 4(b) shows that the electric field is enhanced all along the AgNW when the polarization is perpendicular to the nanowire. The sections b1 and b2 show that the field enhancement is larger at the middle of the nanowire. The b1 section plane shows that more electric field lines terminate at the side than at the top surface of nanowire. This is consistent with the experimental result shown in Fig. 1(b).

It is known that local geometry in the irradiation region can influence the overall field generated by the incident laser beam. After one or more nanoparticles
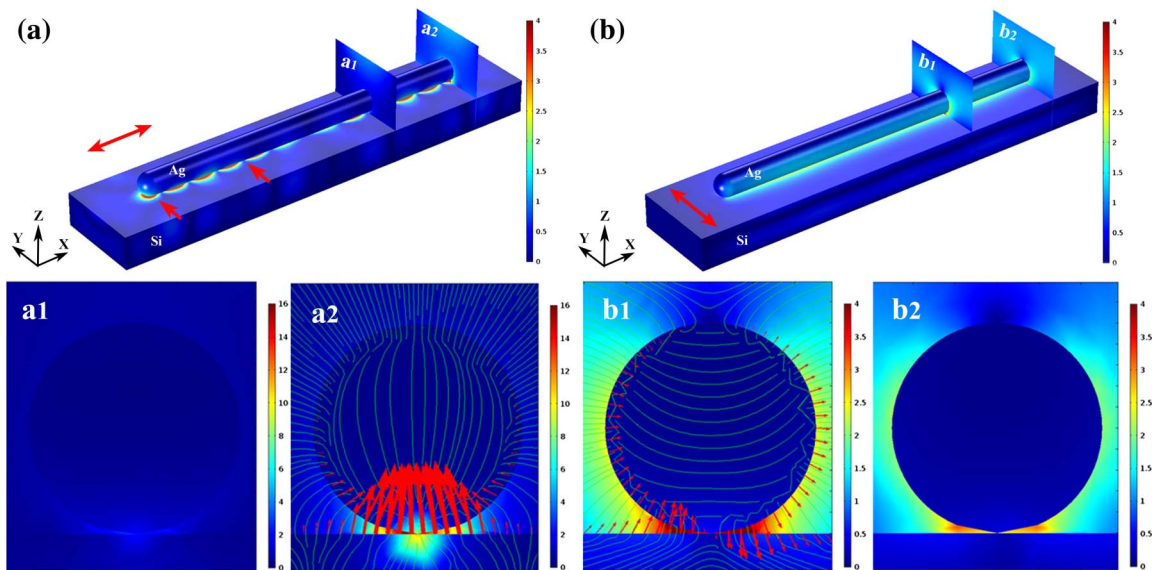
Fig. 4. FEM simulations of the normalized electric field distribution around a single AgNW on a silicon substrate. The laser electric field direction shown by the double-ended arrows. This is parallel to the long axis in (a) and perpendicular to the long axis of the nanowire in (b). The sections at a1 and a2 in (a) are taken at the positions of the single-headed arrows and show the normalized electric field intensities in the y–z plane at locations of low and high field in (a), respectively. The sections b1 and b2 are at the same positions as a1 and a2 but correspond to the fields for perpendicular polarization of the incident laser radiation. The green lines in a2 and b1 show the external electric field lines while red arrows in a2 and b1 show the direction of the electric field at the surface.

become attached to the AgNW, the resulting localized electric field changes and may become enhanced, affecting the subsequent collection and distribution of nanoparticles. Figure 5 shows a simulation of this effect at locations under the nanowire. It is apparent that prior to the accretion of nanoparticles, the electric field distribution is symmetrical along the AgNW and has highest amplitude close to the end of nanowire [Fig. 5(e)]. It is assumed that the nanoparticles move to locations where the field strength is highest. As shown in Figs. 5(a) and 5(c), the introduction of one or two particles on the top of the nanowire surface has little effect on the electric field distribution along the bottom of the nanowire. However, the localized field in the vicinity of these attached nanoparticles is changed. As shown in Figs. 5(b) and 5(d), "hotspots" are generated close to the added AgNPs but these are much weaker than those at the bottom of the wire. Figure 5(e) shows that the regions of strong field enhancement at the bottom of the wire are little affected by additional small particles on the surface of nanowire. It can be concluded that the presence of small particles on the top of the wire only have a limited effect on the distribution of electric field at the bottom of the wire, but can influence the field at their location. Figure 5(e) also reveals that the average separation between the adjacent peaks is ∼130 nm, which is similar to the minimum distance ∼110 nm shown in Fig. 3(a). This suggests that attached particles may influence the position of subsequent particles and the overall distribution of nanoparticles on the AgNW via the generation of "hotspots." Particles are accreted randomly and become spaced as shown in Fig. 3(a). They are separated by multiples of the characteristic distance between "hotspots."
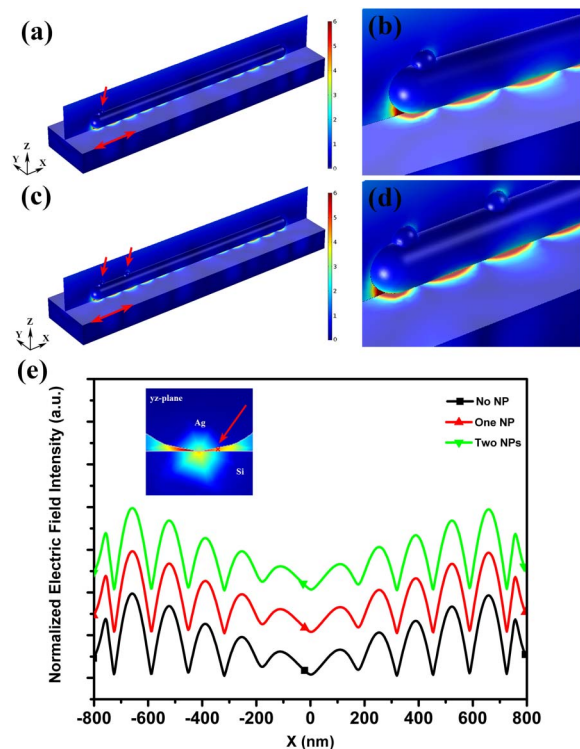

Fig. 5. FEM simulation of the normalized electric field intensity in an AgNW with attached AgNPs. (a) A single AgNP attached at the end of the wire. (c) Two AgNPs as shown on the surface of the AgNW. The single arrows in (a) and (c) show the location of the AgNPs. Double-ended arrows show the direction of polarization in the incident laser beam. (b) and (d) give a magnified image of the field around AgNPs. (e) shows the normalized electric field intensities along the long axis of the nanowire close to lower surface. The location is marked by the cross "x" in the inset.
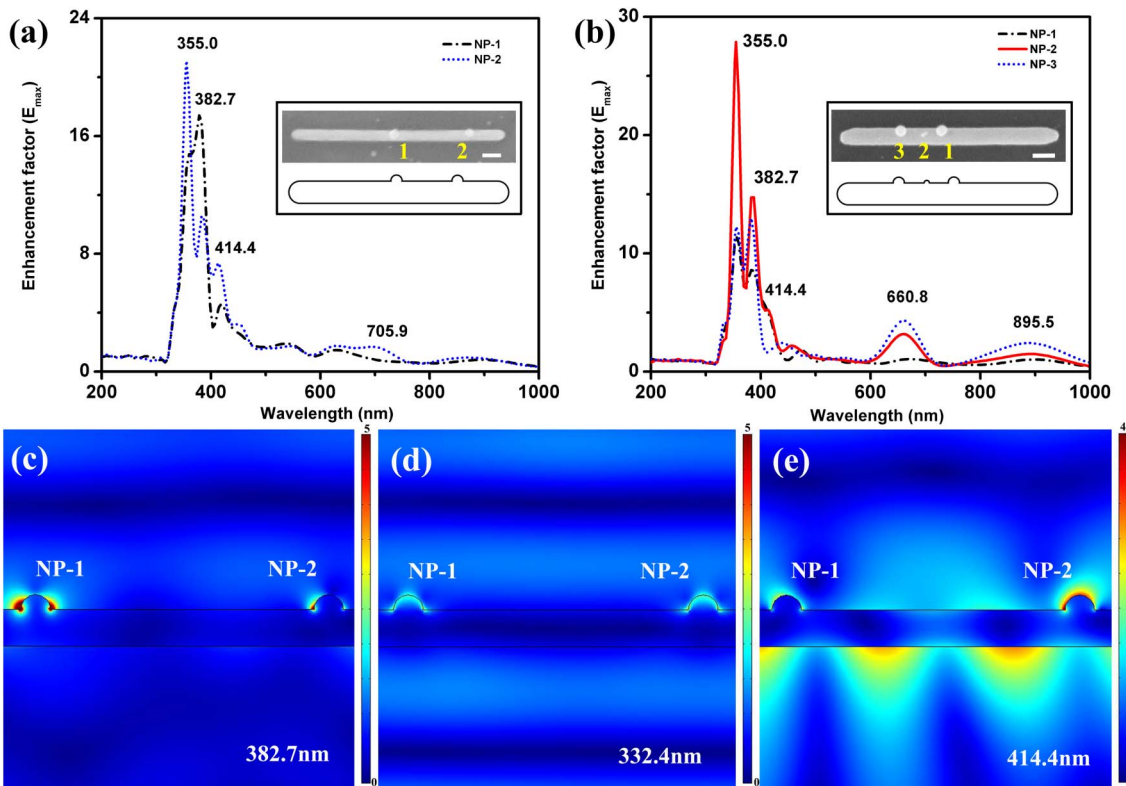
Fig. 6. Maximum enhancement factors of the electric field intensity around some AgNPs attached to a AgNW excited optically at a variety of wavelengths. (a) The wavelength-dependent solution for two AgNPs on an AgNW, nanowire (length = 1120 nm, diameter = 50 nm), NP-1 and NP-2 each have a diameter of 40 nm and are separated by 400 nm. The distance from NP-2 to the end of the nanowire is 200 nm. (b) The solution for three AgNPs on an AgNW (length = 850 nm, diameter = 74 nm). NP-1 and NP-3 are each 42 nm in diameter and NP-2 is 10 nm in diameter. The separation between the NPs is 100 nm, and the distance between NP-3 and the end of the nanowire is 220 nm. Insets in (a) and (b) show the image and schematic of the overall structure, scale bar: 100 nm. The calculated field distribution around NP-1 and NP-2 on optical excitation at wavelengths 382.7, 332.4, and 414.4 nm are shown in (c), (d), and (e), respectively. These solutions are based on the model shown in (a).

C. Optical Properties of Nanostructures

To evaluate potential applications of this assembly technique in the preparation of nanoscale optical logic devices, we have investigated wavelength-dependent electric field enhancement factors for two different AgNP/AgNW configurations. These configurations, shown in the inserts in Figs. 6(a) and 6(b), have been selected from those produced in the present experiments. The first configuration of two AgNPs as shown in Fig. 6(a) consists of two NPs separated by 200 nm, with one particle 200 nm from the right end of a 1120 nm AgNW. The second configuration [Fig. 6(b)], has two 42 nm diameter AgNPs separated by 200 nm with a third 10 nm diameter AgNP midway between them.

The electron density is high in the interconnection region between a nanoparticle and the nanowire connection area because the structural discontinuity enhances the electric field intensity in this volume. As a result, due to the enhancement in electron–photon coupling, those areas can be used as optical antenna. Figure 6 shows the maximum electric field enhancement factors near the attached nanoparticles at different optical excitation wavelengths. These two nanoparticle–nanowire structures were produced by fs laser irradiation as described previously. In Fig. 6(a), the field enhancement at NP-1 is less than at NP-2 at excitation wavelengths of 355.0, 414.4, and 705.9 nm. When the wavelength is changed to 382.7 nm, this situation reverses and the field enhancement at the location of NP-1 is greater than that at NP-2. It can be seen that some excitation wavelengths yield approximately the same field enhancement at both NP-1 and NP-2. The intensity differences near NP-1 and NP-2 at three specific wavelengths are shown in Figs. 6(c)–6(e). By introducing a logical relationship, this structure can then be used as an optical logic processor, for example as a comparator in the electronics industry. Since the resonant wavelength around the antenna is related to nanoparticle size and the overall morphology [35], it is possible to achieve different logical relationships by introducing a range of particles. As an example, the three AgNPs on the AgNW shown in Fig. 6(b), yield a more complex relationship between the field enhancements at various locations, offering the possibility of more complex functionality.

4. Conclusion

Periodic arrays of Ag nanoparticles have been assembled on Ag nanowires using plasmonic effects

induced by 800 nm fs laser radiation. The Ag nanowires were in contact with a silicon substrate and enhancement of the electric field at the nanowire–Si interface is found to be significant in attracting nearby Ag nanoparticles and determines the overall distribution and location of nanoparticles on the nanowire surface. The electric field distribution in this structure is highly dependent on laser polarization. A well-organized array of nanoparticles is favored when the polarization direction is parallel to the long axis of the nanowire. We also find that the array of nanoparticles becomes less organized as the length of the Ag nanowire exceeds twice the laser wavelength. However, some self-organization of Ag nanoparticles is still present even on long nanowires. The collection of nanoparticles has effect on the overall plasmonic field and influences the location and distribution of subsequent nanoparticles on the nanowire. In all cases, the minimum separation between adjacent nanoparticles is ~100 nm. This study suggests that nanoparticles and nanowires can be assembled into well-organized structures using fs lasers, and offers an alternative method of fabricating nanoscaled optical devices such as an optical logic processor.

References

1. S. Zeng, D. Baillargeat, H. Ho, and K. T. Yong, "Nanomaterials enhanced surface plasmon resonance for biological and chemical sensing applications," Chem. Soc. Rev. **43**, 3426–3452 (2014).
2. B. Kenes, M. Rybachuk, J. Hofkens, and H. Uji-I, "Silver nanowires terminated by metallic nanoparticles as effective plasmonic antennas," J. Phys. Chem. C **117**, 2547–2553 (2013).
3. Y. L. Yan, C. Zhang, J. Y. Zheng, J. N. Yao, and Y. S. Zhao, "Optical modulation based on direct photon–plasmon coupling in organic/metal nanowire heterojunctions," Adv. Mater. **24**, 5681–5686 (2012).
4. K. Q. Peng, X. Wang, X. L. Wu, and S. T. Lee, "Platinum nanoparticle decorated silicon nanowires for efficient solar energy conversion," Nano Lett. **9**, 3704–3709 (2009).
5. M. W. Knight, N. K. Grady, R. Bardhan, F. Hao, P. Nordlander, and N. J. Halas, "Nanoparticle-mediated coupling of light into a nanowire," Nano Lett. **7**, 2346–2350 (2007).
6. N. Netzer, R. Gunawidjaja, M. Hiemstra, Q. Zhang, W. Tsukruk, and C. Jiang, "Formation and optical properties of compression-induced nanoscale buckles on silver nanowires," ACS Nano **3**, 1795–1802 (2009).
7. Z. Li, H. Tang, W. Yuan, W. Song, L. Niu, L. Yan, M. Yu, M. Dai, S. Feng, M. Wang, T. Liu, P. Jiang, Y. Fan, and Z. L. Wang, "Ag nanoparticle-ZnO nanowire hybrid nanostructures as enhanced and robust antimicrobial textiles via a green chemical approach," Nanotechnology **25**, 145702 (2014).
8. Z. G. Dai, X. H. Xiao, L. Liao, J. J. Ying, F. Mei, W. Wu, F. Ren, W. Q. Li, and C. Jiang, "Enhanced and polarization dependence of surface-enhanced Raman scattering in silver nanoparticle array-nanowire systems," Appl. Phys. Lett. **102**, 163108 (2013).
9. M. L. Juan, M. Righini, and R. Quidant, "Plasmon nano-optical tweezers," Nat. Photonics **5**, 349–356 (2011).
10. B. J. Roxworthy and K. C. Toussaint, Jr., "Femtoseocond-pulsed plasmonic nanotweezers," Sci. Rep. **2**, 660 (2012).
11. R. J. Berthelot, S. S. Acimovic, M. L. Juan, M. P. Kreuzer, J. Renger, and R. Quidant, "Three-dimensional manipulation with scanning near-field optical nanotweezers," Nat. Nanotechnol. **9**, 295–299 (2014).
12. X. Yang, Y. Liu, R. Oulton, X. Yin, and X. Zhang, "Optical forces in hybrid plasmonic waveguides," Nano Lett. **11**, 321–328 (2011).
13. J. Ndukaife, A. Mishra, U. Guler, A. Nnanna, S. Wereley, and A. Boltasseva, "Photothermal heating enabled by plasmonic nanostructures for electrokinetic manipulation and sorting of particles," ACS Nano **8**, 9035–9043 (2014).
14. L. Cao, R. Nome, J. Montgomery, S. Gray, and N. Scherer, "Controlling plasmonic wave packets in silver nanowires," Nano Lett. **10**, 3389–3394 (2010).
15. H. Ditlbacher, A. Hohenau, D. Wagner, U. Kreibig, M. Rogers, F. Hofer, F. Aussenegg, and J. Krenn, "Silver nanowires as surface plasmon resonators," Phys. Rev. Lett. **95**, 257403 (2005).
16. V. G. Shvedov, A. S. Desyatnikov, A. V. Rode, W. Z. Krolikowski, and Y. S. Kivshar, "Optical guiding of absorbing nanoclusters in air," Opt. Express **17**, 5743 (2009).
17. V. G. Shvedov, C. Hnatovsky, N. Shostka, A. V. Rode, and W. Krolikowski, "Optical manipulation of particle ensembles in air," Opt. Lett. **37**, 1934 (2012).
18. K. Sugioka, J. Xu, D. Wu, Y. Hanada, Z. Wang, Y. Cheng, and K. Midorikawa, "Femtosecond laser 3D micromachining: a powerful tool for the fabrication of microfluidic, optofluidic, and electrofluidic devices based on glass," Lab Chip **14**, 3447 (2014).
19. G. Baffou, R. Quidant, and F. Abajo, "Nanoscale control of optical heating in complex plasmonic systems," ACS Nano **4**, 709–716 (2010).
20. L. Liu, P. Peng, A. Hu, G. Zou, W. Duley, and Y. Zhou, "Highly localized heat generation by femtosecond laser induced plasmon excitation in Ag nanowires," Appl. Phys. Lett. **102**, 073107 (2013).
21. Y. Jiang, T. Narushima, and H. Okamoto, "Nonlinear optical effects in trapping nanoparticles with femtosecond pulses," Nat. Phys. **6**, 1005–1009 (2010).
22. B. Agate, C. Brown, W. Sibbett, and K. Dholakia, "Femtosecond optical tweezers for in-situ control of two-photon fluorescence," Opt. Express **12**, 3011–3017 (2004).
23. A. Plech, V. Kotaidis, M. Lorenc, and J. Boneberg, "Femtosecond laser near-field ablation from gold nanoparticles," Nat. Phys. **2**, 44–47 (2006).
24. M. Huang, F. Zhao, Y. Cheng, N. Xu, and Z. Xu, "Origin of laser-induced near subwavelength ripples: interference between surface plasmons and incident laser," ACS Nano **3**, 4062–4070 (2009).
25. B. Oktem, I. Pavlov, S. Ilday, H. Kalaycioglu, A. Rybak, S. Yavas, M. Erdogan, and F. Ilday, "Nonlinear laser lithography for indefinitely large-area nanostructuring with femtosecond pulses," Nat. Photonics **7**, 897–901 (2013).
26. A. Hu, P. Peng, H. Alarifi, X. Zhang, J. Guo, Y. Zhou, and W. Duley, "Femtosecond laser welded nanostructures and plasmonic devices," J. Laser Appl. **24**, 042001 (2012).
27. A. Hu, G. Deng, S. Courvoisier, O. Reshef, C. Evans, E. Mazur, and Y. Zhou, "Femtosecond laser induced surface melting and nanojoining for plasmonic circuits," Proc. SPIE **8809**, 880907 (2013).
28. B. Wiley, Y. Sun, and Y. Xia, "Synthesis of silver nanostructures with controlled shapes and properties," Acc. Chem. Res. **40**, 1067–1076 (2007).
29. M. Ploschner, M. Mazilu, T. Krauss, and K. Dholakia, "Optical forces near a nanoantenna," J. Nanophoton. **4**, 041570 (2010).
30. P. Ghenuche, S. Cherukulappurath, T. Taminiau, N. van Hulst, and R. Quidant, "Spectroscopic mode mapping of resonant plasmon nanoantennas," Phys. Rev. Lett. **101**, 116805 (2008).

31. V. Miljkovic, T. Shegai, P. Johansson, and M. Kall, "Simulating light scattering from supported plasmonic nanowires," Opt. Express **20**, 10816–10826 (2012).
32. P. Johnson and R. Christy, "Optical constants of noble metals," Phys. Rev. B **6**, 4370 (1972).
33. V. Myroshnychenko, J. Rodriguez-Fernandez, I. Pastoriza-Santos, A. Funston, C. Novo, P. Mulvaney, L. Liz-Marzan, and F. Garcia de Abajo, "Modelling the optical response of gold nanoparticles," Chem. Soc. Rev. **37**, 1792–1805 (2008).
34. C. Galloway, M. Kreuzer, S. Acimovic, G. Volpe, M. Correia, S. Petersen, M. Neves-Petersen, and R. Quidant, "Plamon-assisted delivery of single nano-objects in an optical hot spot," Nano Lett. **13**, 4299–4304 (2013).
35. X. Y. Zhang, T. Zhang, A. Hu, Y. Song, and W. W. Duley, "Controllable plasmonic antennas with ultra narrow bandwidth based on silver nano-flags," Appl. Phys. Lett. **101**, 153118 (2012).